Engineering optical properties of a graphene oxide metamaterial assembled in microfluidic channels

V. G. Kravets,[1,*] O. P. Marshall,[1] R. R. Nair,[1] B. Thackray,[1] A. Zhukov,[1] J. Leng,[2] and A. N. Grigorenko[1]

[1]*University of Manchester, School of Physics and Astronomy, Manchester, UK*
[2]*CNRS, University of Bordeaux, RHODIA, LOF, UMR5258, F-33600, Pessac, France*
[*]*vasyl.kravets@manchester.ac.uk*

Abstract: The dense packing of two dimensional flakes by van der Waals forces has enabled the creation of new metamaterials with desirable optical properties. Here we assemble graphene oxide sheets into a three dimensional metamaterial using a microfluidic technique and confirm their ordering via measurements of ellipsometric parameters, polarized optical microscopy, polarized transmission spectroscopy, infrared spectroscopy and scanning electron microscopy. We show that the produced metamaterials demonstrate strong in-plane optical anisotropy ($\Delta n \approx 0.3$ at $n \approx 1.5$-1.8) combined with low absorption ($k < 0.1$) and compare them with as-synthesized samples of graphene oxide paper. Our results pave the way for engineered birefringent metamaterials on the basis of two dimensional atomic crystals including graphene and its derivatives.

OCIS codes: (160.3918) Metamaterials; (160.4760) Optical properties; (160.1190) Anisotropic optical materials; (350.4600) Optical engineering.

References and links

1. S. A. Maier, *Plasmonics: Fundamentals and Applications* (Springer, New York, 2007).
2. N. Engheta and R. W. Ziolkowski, *Metamaterials, physics and engineering explorations* (IEEE Wiley, New York, 2006).
3. V. G. Kravets, F. Schedin, R. Jalil, L. Britnell, R. V. Gorbachev, D. Ansell, B. Thackray, K. S. Novoselov, A. K. Geim, A. V. Kabashin, and A. N. Grigorenko, "Singular phase nanoparticles in plasmonic metamaterials for label-free single molecule detection," Nat. Mater. **12**(4), 304–309 (2013).
4. D. V. Sivukhin, *Optics* (Nauka, Moscow, 1985).
5. M. Born and E. Wolf, *Principles of Optics* (Cambridge Univ. Press, Cambridge, UK, 1980).
6. A. N. Poddubny, P. A. Belov, P. Ginzburg, A. V. Zayats, and Y. S. Kivshar, "Microscopic model of Purcell enhancement in hyperbolic metamaterials," Phys. Rev. B **86**(3), 035148 (2012).
7. A. V. Kabashin, P. Evans, S. Pastkovsky, W. Hendren, G. A. Wurtz, R. Atkinson, R. Pollard, V. A. Podolskiy, and A. V. Zayats, "Plasmonic nanorod metamaterials for biosensing," Nat. Mater. **8**(11), 867–871 (2009).
8. R. Atkinson, W. R. Hendren, G. A. Wurtz, W. Dickson, A. V. Zayats, P. Evans, and R. J. Pollard, "Anisotropic optical properties of arrays of gold nanorods embedded in alumina," Phys. Rev. B **73**(23), 235402 (2006).
9. G. Eda and M. Chhowalla, "Chemically derived graphene oxide: Towards large-area thin-film electronics and optoelectronics," Adv. Mater. **22**(22), 2392–2415 (2010).
10. E. Morales-Narváez and A. Merkoçi, "Graphene oxide as an optical biosensing platform," Adv. Mater. **24**(25), 3298–3308 (2012).
11. T. F. Yeh, J. Cihlar, C. Y. Chang, C. Cheng, and H. Teng, "Roles of graphene oxide in photocatalytic water splitting," Mater. Today **16**(3), 78–84 (2013).
12. R. R. Nair, H. A. Wu, P. N. Jayaram, I. V. Grigorieva, and A. K. Geim, "Unimpeded permeation of water through helium-leak-tight graphene-based membranes," Science **335**(6067), 442–444 (2012).
13. R. R. Nair, H. A. Wu, P. N. Jayaram, I. V. Grigorieva, and A. K. Geim, "Unimpeded permeation of water through helium-leak-tight graphene-based membranes," Science **335**(6067), 442–444 (2012).
14. T. Gokus, R. R. Nair, A. Bonetti, M. Böhmler, A. Lombardo, K. S. Novoselov, A. K. Geim, A. C. Ferrari, and A. Hartschuh, "Making graphene luminescent by oxygen plasma treatment," ACS Nano **3**(12), 3963–3968 (2009).

#224766 - $15.00 USD Received 15 Oct 2014; revised 9 Jan 2015; accepted 9 Jan 2015; published 20 Jan 2015

15. P. Massé, S. Mornet, E. Duguet, M. Tréguer-Delapierre, S. Ravaine, A. Iazzolino, J.-B. Salmon, and J. Leng, "Synthesis of size-monodisperse spherical Ag@SiO2 nanoparticles and 3-D assembly assisted by microfluidics," Langmuir **29**(6), 1790–1795 (2013).
16. A. Merlin, J.-B. Salmon, and J. Leng, "Microfluidic-assisted growth of colloidal crystals," Soft Matter **8**(13), 3526–3537 (2012).
17. A. Baron, A. Iazzolino, K. Ehrhardt, J.-B. Salmon, A. Aradian, V. Kravets, A. N. Grigorenko, J. Leng, A. Le Beulze, M. Tréguer-Delapierre, M. A. Correa-Duarte, and P. Barois, "Bulk metamaterials at optical frequencies assembled by microfluidic evaporation," Opt. Mater. Express **3**, 1792–1797 (2013).
18. W. S. Hummers, Jr. and R. E. Offeman, "Preparation of graphitic oxide," J. Am. Chem. Soc. **80**(6), 1339 (1958).
19. R. K. Joshi, P. Carbone, F. C. Wang, V. G. Kravets, Y. Su, I. V. Grigorieva, H. A. Wu, A. K. Geim, and R. R. Nair, "Precise and ultrafast molecular Sieving through graphene oxide membranes," Science **343**(6172), 752–754 (2014).
20. A. K. Geim and I. V. Grigorieva, "Van der Waals heterostructures," Nature **499**(7459), 419–425 (2013).
21. P. V. Kumar, N. M. Bardhan, S. Tongay, J. Wu, A. M. Belcher, and J. C. Grossman, "Scalable enhancement of graphene oxide properties by thermally driven phase transformation," Nat. Chem. **6**(2), 151–158 (2013).
22. H. Feng, R. Cheng, X. Zhao, X. Duan, and J. Li, "A low-temperature method to produce highly reduced graphene oxide," Nat. Commun. **4**, 1539–1545 (2013).
23. L. Yang, J. Deslippe, C. H. Park, M. L. Cohen, and S. G. Louie, "Excitonic effects on the optical response of graphene and bilayer graphene," Phys. Rev. Lett. **103**(18), 186802 (2009).
24. V. G. Kravets, A. N. Grigorenko, R. R. Nair, P. Blake, S. Anissimova, K. S. Novoselov, and A. K. Geim, "Spectroscopic ellipsometry of graphene and an exciton-shifted van Hove peak in absorption," Phys. Rev. B **81**(15), 155413 (2010).
25. I. Jung, M. Vaupel, M. Pelton, R. Piner, D. A. Dikin, S. Stankovich, J. An, and R. S. Ruoff, "Characterization of thermally reduced graphene oxide by imaging ellipsometry," J. Phys. Chem. C **112**(23), 8499–8506 (2008).
26. V. G. Kravets, F. Schedin, S. Taylor, D. Viita, and A. N. Grigorenko, "Plasmonic Resonances in Optomagnetic Metamaterials Based on Double Dot Arrays," Opt. Express **18**(10), 9780–9790 (2010).
27. L. J. Cote, F. Kim, and J. Huang, "Langmuir-Blodgett assembly of graphite oxide single layers," J. Am. Chem. Soc. **131**(3), 1043–1049 (2009).
28. J. N. Israelachvili, *Intermolecular and surface forces* (2nd ed.; Academic Press: San Diego, 1992, p. 450).

1. Introduction

Developments in the fields of electromagnetic metamaterials (MMs) and plasmonic optics have provided the means to design optical structures with a variety of desirable characteristics [1–3]. This has given rise to engineered materials with tailored effective refractive indexes ranging from positive to negative values. Artificial optical MMs could deliver optical devices with smaller sizes, wider spectral range and better tunability. One of the oldest materials, that is still extremely important for various applications, is an anisotropic (birefringent) optical medium. Indeed, birefringent materials were discovered by Rasmus Bartholin in 17th Century and were successfully used in a multitude of important optical devices, such as beam-splitters, polarizers (e.g., Nicole and Glan-Thomson prisms), wave plates, light modulators, phase matching elements, etc [4,5]. Natural birefringent materials normally do not possess strong anisotropy: the typical difference between ordinary and extraordinary indices of refraction in anisotropic crystals, Δn, is below 0.1 (with exceptions of commonly used calcite $CaCO_3$, Δn = 0.17, and rare rutile TiO_2 which has extremely large refractive index of 2.9 and Δn = 0.28) [4,5]. At the same time, the task of miniaturising requires birefringent materials with higher values of optical anisotropy. This task can be solved with the help of artificial (man-made) metamaterials.

There are several approaches to creating metamaterials with large optical anisotropy. For example, MMs may be designed by stacking sub-wavelength structures [6], or by exploiting the dispersion characteristics of composite metal-dielectric waveguides [7,8]. We made use of another emerging technology: microfluidic self-assembly of nanostructures into a densely packed 3D metamaterial. To demonstrate the feasibility and potential of this technique we have chosen semiconductor-like graphene oxide (GO) as building blocks for 3D metamaterials. The reason for this choice is two-fold: first, graphene oxide is a promising material for a variety of optical applications, see the review [9], and second, in contrast to graphene, it possesses reasonably low absorption which is important for practical devices. Graphene oxide is particularly attractive to researchers due to the abundance of oxygen-containing groups on the graphene nanosheets, enabling stable dispersion in water and

#224766 - $15.00 USD Received 15 Oct 2014; revised 9 Jan 2015; accepted 9 Jan 2015; published 20 Jan 2015

chemical modification. Numerous GO applications have already been explored such as biosensing [10], photocatalysis [11], electronics and optoelectronics [9], amongst others. Composite materials derived from graphene (such as GO), with novel or enhanced properties and functions, have also been extensively studied recently [12–14].

A recently developed microfluidic evaporation technique is described in detail elsewhere [15–17]. It allows one to concentrate within a micron-sized channel any type of solute initially dispersed in water thanks to a semi-permeable membrane across which water can evaporate, but not solutes. In a dead-end geometry filled with a dilute solution or dispersion, the concentration of solute increases first at the tip of the capillary until a dense state nucleates, the latter then grows and invades the linear channel geometry. The main advantages of the microfluidic design are i) to control the concentration rate, and ii) to improve optical properties of the assembled structures by tuning geometry of elements ordering and providing metamaterials with excellent quality of surfaces (low roughness and high homogeneity). A variety of optical metamaterials can be formed from colloidal nanostructures assembled in this way. For instance, the authors recently described 3D metamaterials produced by microfluidics from densely packed Au nanospheres (or Ag nanocubes) which can exhibit high refractive indices in the visible and near IR region [17].

In this work, we demonstrate birefringent 3D metamaterials made from flakes of 2D atomic crystals (graphene oxide) by microfluidic technique. The fabricated materials show a large value of optical in-plane anisotropy, $\Delta n \approx 0.3$ at $n \approx 1.5\text{-}1.8$, and low absorption, $k < 0.1$, in a wide spectral range from the visible to the near-infrared (NIR). The effective dielectric functions of GO sheets assembled in microfluidic channels and directly deposited on a quartz substrate were extracted using spectroscopic ellipsometry. The geometry, size and volume fraction of the GO sheets in water solution, for assembly within the microfluidic channels, constitute degrees of freedom to engineer the desired index of refraction and desired anisotropy. Furthermore, an important feature of our fabrication technique is that the resulting MMs are conveniently contained inside microfluidic channels, ready to be used in a fabrication of bulk optical devices. The precise values of refractive indices in the proposed anisotropic dielectric 3D MMs are sensitive functions of the gap width between packed nanostructures. Our work provides an insight into three areas: (1) understanding the fundamental behavior of assembled GO films, (2) exploration of the feasibility of GO film-based optoelectronics, and (3) identification of the key issues in the formation of dense packed GO sheets in microfluidics. Large-scale alignment of GO sheets within microfluidic channels observed in our experiments opens the way to ordered structures of graphene-based functional materials, and offers the prospect of new optical phenomena.

2. Sample preparation and characterization

Graphite oxide was prepared by exposing millimeter size flakes of natural graphite to concentrated sulfuric acid, sodium nitrate and potassium permanganate (Hummers' method) [18,19]. Then, graphite oxide was exfoliated into monolayer flakes by sonication in water, which was followed by centrifugation at 10,000 rpm to remove any remaining few-layer crystals. The resulting GO flakes were mostly single layered (flake thickness ~1.0 nm) with lateral dimensions of 500-1500 nm, as characterized by scanning electron microscopy (SEM) (Fig. 1(a)). The modified Hummers method produced a GO suspension which was yellow/light brown in color, indicating that the carbon lattice structure was distorted by the added oxygenated functional groups; pure graphene or graphite is black. The GO nanosheets were extremely hydrophilic, remaining suspended in water for several months without signs of aggregation or deposition.

We describe results obtained on three different microfluidic chips, each with water as the base fluid but with GO flake concentrations of 0.2, 0.3 and 0.5 mg/ml. These GO solutions were measured in their initial state using optical techniques to understand how concentration impacts the bonding between the primary constituent atoms, i.e. by studying the C-C, C-O

#224766 - $15.00 USD Received 15 Oct 2014; revised 9 Jan 2015; accepted 9 Jan 2015; published 20 Jan 2015

and C-OH electronic and vibrating resonances. Each channel on the microfluidic chip was 100 μm wide, h = 10 μm deep and several millimeters long. Such device architecture enabled the assembly of densely packed nanostructures from the input GO solution.

The optical properties of the GO nanosheets and GO-based microfluidics were characterized by Raman spectroscopy (Witec), Fourier transform infrared (FTIR) spectroscopy (Bruker, Vertex 80) combined with an infrared microscope, and scanning electron microscopy (SEM). Transmission of *p*- and *s*- polarized light was measured at normal incidence using an Ocean Optics USB2000 spectrometer. Light from a xenon source was passed through a polarizer and then focused on to the surface of the sample to a spot approximately 100 μm in diameter. The transmitted light was collected using an optical fiber coupled to the spectrometer (200 μm core).

The spectrally dependent refractive indices and extinction coefficients of multiple-layer GO samples (pure GO flakes) and microfluidic-assembled dense packed GO were extracted by variable angle spectroscopic ellipsometry (J.A. Woollam Co., Inc., M-2000F) in the wavelength range of 240-1700 nm and were compared to previously reported GO sheet measurements. Dispersion functions for the dense packed GO sheets were also compared to those obtained by standard spectroscopic ellipsometry of many overlapping deposited GO layers. Differences were observed in both the concentration of the GO deposits and in the dispersion parameters. A model is proposed to explain these observations, based on the self assembly of dense packed GO sheets in the microfluidic channels.

3. Results and discussion

For SEM imaging and optical characterization of the initial GO nanosheets, small volumes of diluted GO suspension were deposited on smooth quartz substrates and then dried before measurement. The SEM image in Fig. 1a reveals a layer-by-layer assembly of GO sheets, confirming the face-to-face nature of the interaction between GO flakes due to van der Waals attractions [20]. The structural model of single layer GO in Fig. 1(b) shows the hexagonal network of covalently linked carbon atoms, with oxygen-containing functional groups attached to various sites. Interactions between the constituent atoms provide rich optical spectra, with both Raman and IR active modes. Raman spectra (Fig. 1(c)) show the G peak at ~1590 cm^{-1} stemming from the sp^2 hybridization of graphitic carbon, and the D peak at ~1350 cm^{-1} confirming distortion of the carbon lattice (the appearance of atomic scale defects on the graphene lattice). As the GO solution concentration is increased the double-resonance band (2D) becomes more pronounced whereas the ratio of the D and G peak intensities remains approximately constant.

Figure 1(d) shows the FTIR spectra measured in reflection mode, with signatures of unoxidized sp^2 C = C bonds in the carbon lattice (~1571 cm^{-1}) and oxygen-containing functional groups: C–OH vibration (~1225 cm^{-1}), weak C-O-H bending vibration (~1410 cm^{-1}), and C = O stretching vibration (~1721 cm^{-1}), which have all been observed previously [21,22]. In addition, a strong band is present at ~1055 cm^{-1}, which is attributed to the stretching vibration of C-O. FTIR spectroscopy also reveals the existence of water (O-H) functional groups (~3400 cm^{-1}). It is worth noting that the main features in the FTIR spectra exhibit a shift to smaller wavenumbers with increased GO solution concentrations.

The absorption spectra for GO sheets shown in Fig. 1(e) reveals a flat shape for wavelengths λ>600nm. However, there is a strong deviation from this trend in the blue and UV regions, where absorption rises rapidly. For the highest GO concentration a peak in absorption occurs at λ~315nm. This is due to the fact that the electronic spectrum of GO is nonlinear at energies close to the bandgap of semiconductor-like sheets and exhibits a van Hove singularity in the density of states [23]. The shift to longer wavelength and asymmetry of this peak is the result of excitonic effects [23, 24].

#224766 - $15.00 USD Received 15 Oct 2014; revised 9 Jan 2015; accepted 9 Jan 2015; published 20 Jan 2015

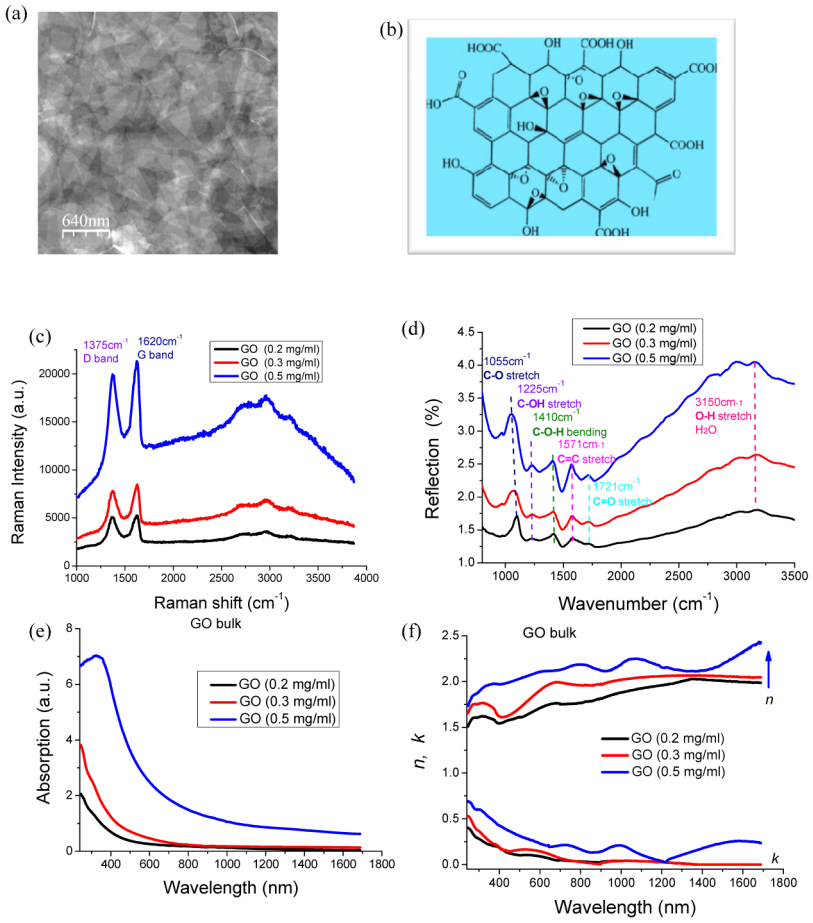

Fig. 1. Droplet assembly of overlapping graphene oxide flakes. (a) SEM image of GO flakes. (b) Structural model of GO sheets indicating the presence of oxygen-containing functional COOH groups. (c) Raman spectra for dried GO solution measured for different concentrations (laser wavelength 514.5 nm). (d) FTIR spectra of overlapping GO flakes as a function of concentration. (e) Changes in optical absorption of GO due to oxidization. (f) Reconstructed optical constants of overlapping GO flakes.

Effective refractive indexes (real and imaginary) of stacked graphene oxide sheets, approximately 100nm thick, were measured by standard spectroscopic ellipsometry. The values of both n and k were observed to increase with GO concentration (Fig. 1(f)). The measured spectra could, of course, be influenced by excitonic effects in the UV region (spectral features are present in n and k at λ~315nm). Peaks in k observed in the region between 1000 and 1200 nm are related to water absorption. Note that GO based materials remain partially absorbing even at energies below the bandgap energy. This additional absorption can be attributed to microscopic scattering at the GO sheet edges and to a pure graphene contribution due to the existence of partially non-oxidized flakes.

The main results of our research are presented in Figs. 2 and 3, which show the evolution of the GO sheet optical properties due to their assembly in microfluidic channels. Figures 2 (a-b) show transmission spectra for the GO microfluidic chips for p- and s-polarized light (relative to the long axis of the microchannels), at an incident angle of $\theta = 0$. Measurements were taken along the length of the microchannels. The resulting spectra all display a similar form, transmission increases towards longer wavelengths. However, the transmission values for p-polarized light are smaller than for s-polarized light by up to ~5-7% in the wavelength

#224766 - $15.00 USD Received 15 Oct 2014; revised 9 Jan 2015; accepted 9 Jan 2015; published 20 Jan 2015

range 350-1000nm. Note also that in the middle section of the microchannel this difference is smaller (2-3%) than for GO sheets at the end (or tip) of the channels. In order to confirm this behavior samples were also studied using FTIR spectroscopy (Fig. 2(c)). These independent measurements confirm the polarization dependence of the transmission spectra and also revealed the influence of GO concentration. In the case of high concentration (0.5 mg/ml) the transmission is very sensitive to the polarization of probing light, whereas for smaller concentrations (0.2, 03 mg/ml) we see negligible differences for *p*– and *s*–polarized light. Note that enhanced anisotropic behavior occurs for assembled GO sheets in a wavelength range covering the visible to the near IR (Fig. 2(c)).

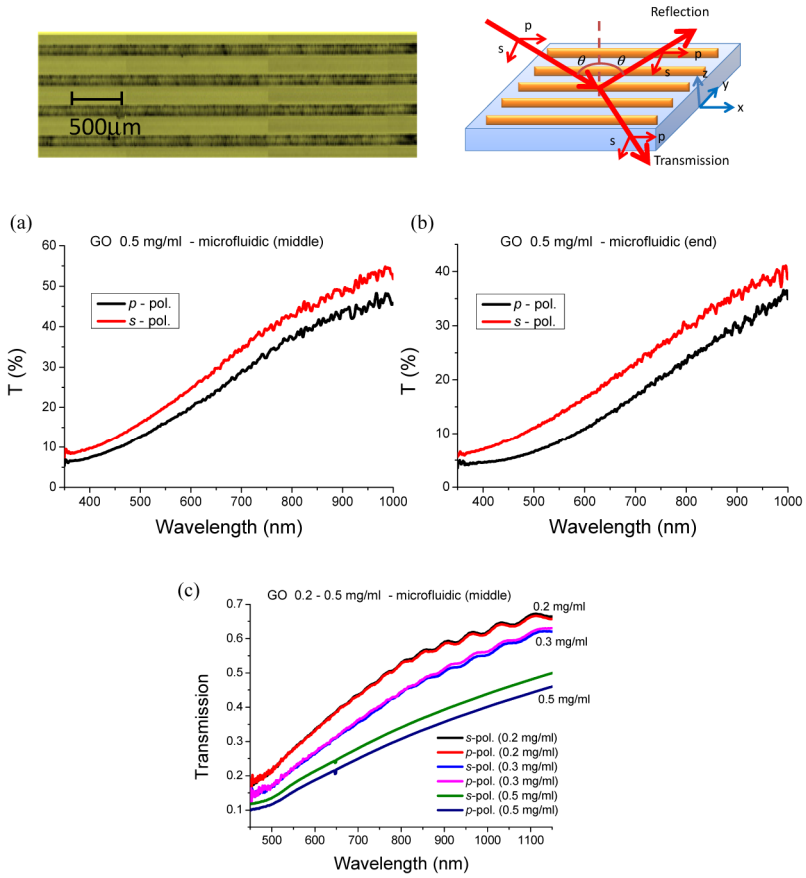

Fig. 2. Evolution of the optical properties of graphene oxide sheets along microfluidic channels. (a,b) Polarized transmission spectra for dense packed GO sheets in microfluidics taken from different areas of microchannel. (c) Anisotropic properties of assembled GO sheets are confirmed by FTIR spectrometry. Inset (a): Optical image of microfluidic channels. Inset (b): Schematic of the ellipsometric and polarized transmission measurements.

Ellipsometric spectra of the GO sheets assembled in microfluidics are shown in Fig. 3(a) for angles of incidence from 50 −70°. It is clear from the transmission behavior presented in Fig. 2 that an isotropic model cannot be used to fit the measured ellipsometric function effectively for assembled GO sheets. Based on this fact we applied an anisotropic model which gave an excellent fit to the measured data (dashed lines in Fig. 3(a)). Minima and maxima in the ellipsometric function of Psi appear at different wavelengths dependent upon the incident angle. This is attributed to an interference resonance and is confirmed by calculation. The optical properties of such anisotropic 3D materials (with in-plane anisotropy) can be characterized by two complex indices of refraction $n_x + ik_x$ and $n_y + ik_y$, and a direction

#224766 - $15.00 USD Received 15 Oct 2014; revised 9 Jan 2015; accepted 9 Jan 2015; published 20 Jan 2015

for the optic axis. For microfluidic assembled GO we choose a coordinate system such that the x axis is in the plane of incidence (along the longitudinal axis of the channel), the y axis is perpendicular to the plane of incidence (perpendicular to channel, transverse direction) and the z axis pointing out of the microchannels. If the optic axis is in the y direction, then $n_x = n_z = n_o$ and $n_y = n_e$ (analogous with crystal optics, n_o is an ordinary index of refraction, and n_e corresponds to an extraordinary index of refraction). In this coordinate system the electric field of s-polarized light lies only in the y axis and hence experiences only n_o. Complex refractive indices were obtained by a fitting procedure minimizing the mean square error (MSE) between the model and experimental data. In this work the data fitting was performed with the WVASE32 software. The resulting complex (anisotropic) refractive indices for the assembled GO sheets in microfluidics are shown in Fig. 3(b). The features of the fitting results resemble those of the thick GO films (Fig. 1(f)). In the near IR region above 1000 nm the values for n_x and n_y are nearly constant, and k_x and k_y are close. The increase in k_x in the UV region can be attributed to bandgap absorption in semiconductor-like GO sheets. Moreover, the increase in k_y can be associated with scattering of light at the edges of dense packed sheets. It is worth noting that the extinction coefficient of ~0.2 at 400 nm obtained here is smaller than those of graphite which typically has values around 1.3-1.5 and single layer graphene around 1.1-1.3 [24], but is close to that of thin reduced GO 'stacks' obtained by heating at 200° C, where k ~0.55 [25]. Thus the obtained results show that the optical response of GO sheets assembled in microfluidics can be considered as that of an anisotropic layer composed of dense packed intrinsically isotropic GO constituents.

For dense packed GO sheets in microfluidic channels we observe by eye a marked change in color using a polarized microscope. Figures 3(c) and 3(d) show polarization-contrast optical microscopy images for reflected TE (s-polarization) and TM (p-polarization) light respectively. We see that the reflection from our sample is highly sensitive to polarization; a clear and simple confirmation of the anisotropy of the investigated 3D microstructures. For polarization along the channel, light mainly interacts with the larger refractive index regions (curve n_x Fig. 3(b), TM image Fig. 3(d)). On the other hand, if the polarization is across the sheets the light experiences a lower effective index from the average of two materials: GO sheets and air (curve n_y Fig. 3(b), TE image Fig. 3(c)). We suggest that this birefringence (anisotropy) arises from the assembled shape of the packed microstructures rather than from any intrinsic property of the constituent GO-like material. The difference between the two effective indices gives a measure of the birefringence Δn. In the case studied here, we obtained a birefringence of Δn = 0.1-0.3 for the visible and near IR spectral regions. This value is sensitive to the concentration of GO and increases monotonically with wavelength, until it becomes limited by the finite size of the structure.

In order to perform the interferometric measurements we used the fringe mode of a home-made Mach-Zehnder interferometer, described in detail in our recent work [26]. The green laser light (λ = 543nm) propagated through assembled GO flakes in microfluidics, in both p- and s-polarizations. Comparing interference fringes generated with (Figs. 3(e) and (f)) and without the sample we directly inferred the phase shift for each polarization and the difference between them. In order to perform this measurement part of the GO microfluidic was separated from the polymer substrate on the glass substrate. This thick, inhomogeneous polymer layer is sensitive to deformation and prohibited accurate phase measurements. A phase difference $\Delta\varphi$ is extracted from the interferograms for p- and s- polarized light and this difference can be described by $\Delta\varphi = 2\pi(\Delta n d)/\lambda$, where Δn is the difference between two effective indices of refraction ($\Delta n_{eff} = n_x - n_y$) and d is the thickness of the GO filled microfluidic. The average measured phase difference (due to the anisotropic behaviour of the assembled GO flakes in microfluidics) was $\Delta\varphi$ = 13, a result of the interferences between air/GO-flakes and GO-flakes/glass. Setting d≈150nm and $\Delta\varphi$ = 13° in the equation above we calculate Δn≈0.13 for green light. Thus the effective birefringence Δn determined from

#224766 - $15.00 USD Received 15 Oct 2014; revised 9 Jan 2015; accepted 9 Jan 2015; published 20 Jan 2015

ellipsometric (Fig. 3(b)) and interferometric (Figs. 3(e) and (f)) data are in agreement with each other.

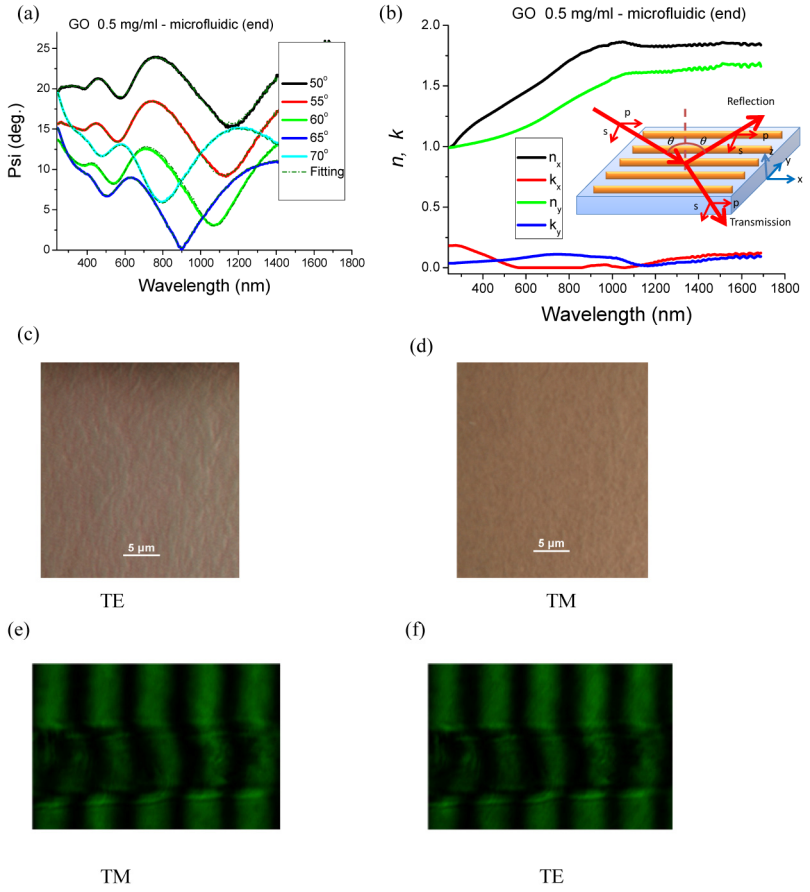

Fig. 3. Variable angle spectroscopic ellipsometry of self assembled GO sheets in microfluidics. (a) Psi spectra of dense packed GO flakes in microfluidics for different angles of incidence. Dashed curves are fits based on Fresnel equation calculations). (b) Extracted anisotropic optical constants of assembled GO sheets in microfluidics. (c,d) Polarization-contrast optical microscopy images (reflection mode) for assembled GO sheets in microfluidics. (e,f) Examples of typical measured interferograms of assembled GO flakes in microfluidics for TM and TE light at λ = 543 nm.

These results raise a number of interesting questions, with one above all others: Why do GO sheets assembled in microfluidics show significant alteration of their optical properties, from isotropic to anisotropic behavior? To answer this question, it is important to know how atomically thin GO flakes assemble in microfluidics and how they behave due to interaction with one another. In an attempt to answer this question an investigation was carried out into the fundamental behavior of dense packed GO microstructures. The Raman spectra in Fig. 4(a) show an evolution along the length of microchannel as the GO sheet assembly occurs. Prominent D and G peaks are present as for pure GO flakes (Fig. 1(c)), indicating a lack of changes at the atomic scale in terms of bonding or the stability of the GO lattice. FTIR spectroscopy was also used to characterize the assembled GO sheets in microfluidics (Figs. 4(b) and (c)). Spectra collected from different sections of the microchannel are practically identical in terms of the identifiable spectral bands, as expected from the Raman measurements. These bands indicate the presence of oxygen-containing functional COOH groups and correspond to the C–O–H deformation vibration and the C–O, C–OH, C = C and

#224766 - $15.00 USD Received 15 Oct 2014; revised 9 Jan 2015; accepted 9 Jan 2015; published 20 Jan 2015

C = O stretching vibrations. The most prominent features are in accordance with FTIR measurements of GO sheets (Fig. 1(d)). The main FTIR peaks are shifted slightly to lower wavenumbers in the microfluidic assembled GO sheets (Figs. 4(b) and (c)). The reproducible feature we used to distinguish between GO in its free and microfluidic assembled states is a stronger reflectivity peak from the C = C stretching vibration at 1560-1575 cm^{-1} (inset Fig. 4(c)). Its behavior is different from that observed for the C-O stretching vibration at 1055 cm^{-1}, which always remained strong. The layered nature of the van der Waals forces in the assembled GO sheets determines both the wavenumber and amplitude of the FTIR spectral features. The increased peak intensity around 1570 cm^{-1} in dense packed GO flakes is attributed to the rising prominence of the C = C bond.

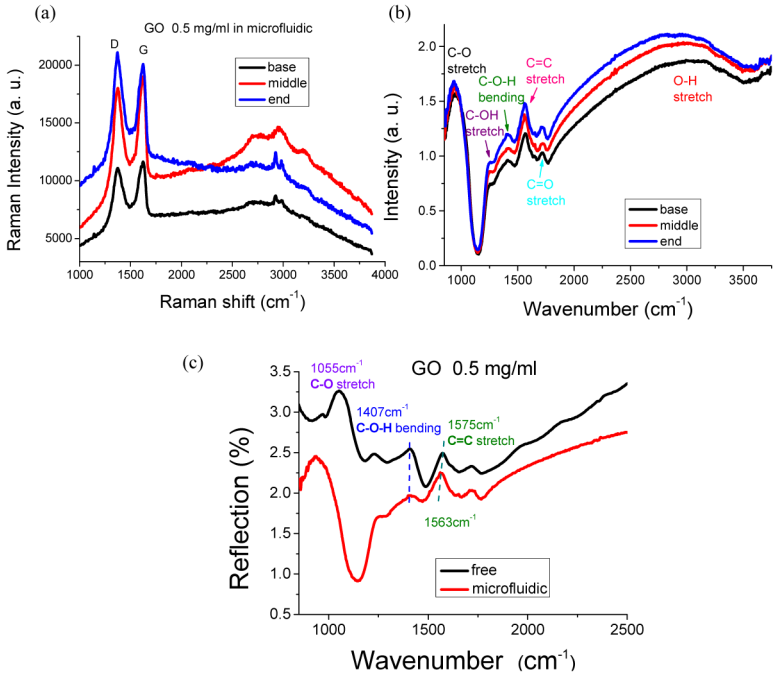

Fig. 4. Optical properties of dense packed GO sheets in microfluidics. (a) Comparison of Raman spectra of dense packed GO flakes in microfluidics taken from different channel sections (analogous to Fig. 1(c)). (b) FTIR spectra of assembled GO flakes in microfluidics. (c) FTIR reflection spectra differ for GO sheets in their free (black) and microfluidic assembled (red) states.

The local orientation of the GO flakes in microfluidics can be directly visualized by SEM. In Figs. 5(a) and 5(b) we compare SEM images of overlapping GO sheets as prepared from dried solution and GO sheets assembled in microfluidics respectively. For the prepared sample, overlapping GO flakes, aligned parallel to the substrate surface, are clearly visible. In comparison, the dense packed GO sheets assembled in the microfluidic channel are aligned along the channel axis. Blocks (domains) of collectively oriented GO sheets are observed, with smooth domain bends along the channel direction.

#224766 - $15.00 USD Received 15 Oct 2014; revised 9 Jan 2015; accepted 9 Jan 2015; published 20 Jan 2015

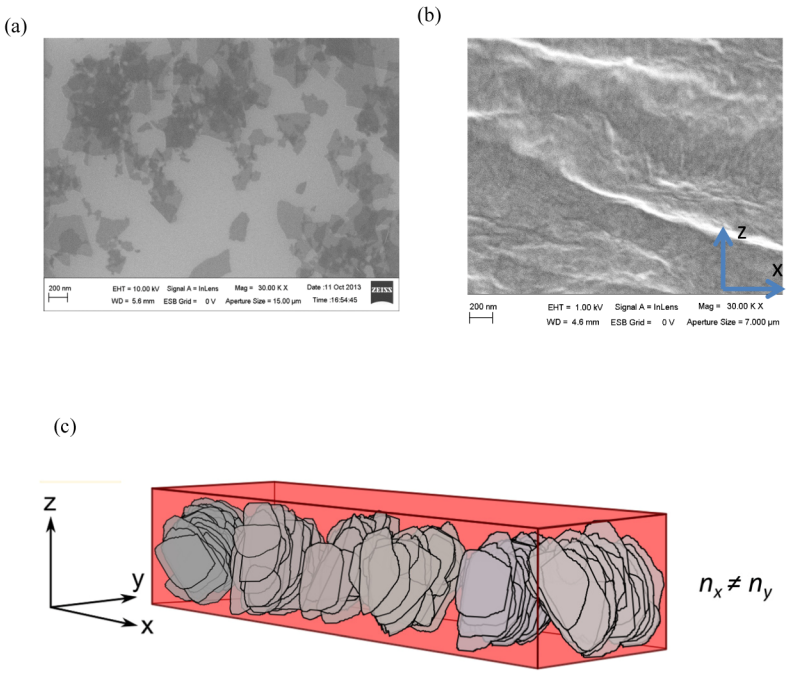

Fig. 5. SEM images showing flake-by-flake assembly of GO sheets. (a) Overlapping GO sheets resulting from dried solution. (b) GO sheets assembled in microfluidics revealing aligned domains along the microchannel axis. (c) Proposed model for the organized assembly of dense packed GO in microfluidics.

It is known that GO forms a colloidal solution in water due to electrostatic repulsion between the ionized carboxylic and phenol hydroxyl groups [27]. These groups are located mainly at the edges of flakes and so are the charges. When several GO sheets approach each other they experience both electrostatic repulsion and van der Waals attraction. Note that the scaling law of van der Waals potential versus separation ($1/d^n$) depends on the size of the interacting bodies [27]. If the GO sheets are brought together in a flake-to-flake manner (as illustrated in Fig. 5(c)) their van der Waals potential can scale as $1/d^2$ [27,28]. Such flake-to-flake interactions also depend on the relative sizes of the sheets. The size distribution of GO flakes along the microfluidic channels is a complex question. From the one hand, the largest flakes get concentrated more quickly than the small ones because they are less prone to diffusion which counteracts the flow. On the other hand, traces of salt get concentrated as well, although slowly as salt diffuses quickly. These may explain why the aspect of the material is different at the tip of the capillary: van der Waals interactions are balanced by electrostatic ones which depend on the amount of added salt. Therefore, we may expect that at the tip of the capillary, the state of dense GO is different than in the rest of the capillary and could lead to neatly stacked GO flakes forming dense packed blocks (domains). In close-packed GO sheets the gaps between GO sheets are too small to resolve using our SEM, but we do see packed block edges (Fig. 5(b)).

4. Conclusions

Three dimensional metamaterials made of graphene oxide flakes by the microfluidic self-assembly technique for optoelectronic applications have been demonstrated. We studied these materials optically and structurally and compared their properties to the properties of GO paper and individual GO flakes. The spectral response of our metamaterials shows pronounced birefringence revealed by variable angle spectroscopic ellipsometry, transmission

#224766 - $15.00 USD Received 15 Oct 2014; revised 9 Jan 2015; accepted 9 Jan 2015; published 20 Jan 2015

measurements and polarized FTIR spectroscopy. The high value of anisotropy, $\Delta n \approx 0.3$, low absorption, $k < 0.1$, readiness to be used for fabrication of bulk devices and broad working spectral range make microfluidic metamaterials useful for possible applications in beam-splitters, polarizers, wave plates, light modulators, etc. The morphology of the assembled GO sheets in microfluidics reveals a well-packed structure with a flake-by-flake connection facilitated by van der Waals interactions. The suggested technique can be applied to fabricate 3D metamaterials from other 2D atomic crystals including graphene, graphene derivatives, boron-nitride and transition metal chalcogenides.

Acknowledgments

The work was supported by European Commission under Graphene Flagship (contract no. CNECT-ICT-604391), Samsung SAIT GRO programme, Bluestone Global Tech grant. ANG acknowledges the amicable hospitality of the University of Bordeaux invited professorship scheme.

#224766 - $15.00 USD Received 15 Oct 2014; revised 9 Jan 2015; accepted 9 Jan 2015; published 20 Jan 2015